NANOPHOTONICS

Three-dimensional cross-nanowire networks recover full terahertz state

Kun Peng[1], Dimitars Jevtics[2], Fanlu Zhang[3], Sabrina Sterzl[1], Djamshid A. Damry[1], Mathias U. Rothmann[1], Benoit Guilhabert[2], Michael J. Strain[2], Hark H. Tan[3], Laura M. Herz[1], Lan Fu[3], Martin D. Dawson[2], Antonio Hurtado[2], Chennupati Jagadish[3], Michael B. Johnston[1]*

Terahertz radiation encompasses a wide band of the electromagnetic spectrum, spanning from microwaves to infrared light, and is a particularly powerful tool for both fundamental scientific research and applications such as security screening, communications, quality control, and medical imaging. Considerable information can be conveyed by the full polarization state of terahertz light, yet to date, most time-domain terahertz detectors are sensitive to just one polarization component. Here we demonstrate a nanotechnology-based semiconductor detector using cross-nanowire networks that records the full polarization state of terahertz pulses. The monolithic device allows simultaneous measurements of the orthogonal components of the terahertz electric field vector without cross-talk. Furthermore, we demonstrate the capabilities of the detector for the study of metamaterials.

The terahertz (THz) band (0.1 to 30 THz) of the electromagnetic spectrum is where electronics meets optics, with THz photons sharing properties from the neighboring spectral regions. For example, in common with microwaves, THz radiation is non-ionizing and penetrates through most nonconducting materials, yet THz radiation can be directed by optical components similar to infrared light. This mixed property enables a wide variety of THz applications, including wireless communication, spectroscopy, sensing, and imaging (*1*).

Time-domain spectroscopy (TDS) with single or subcycle pulses of THz radiation is a powerful tool for materials characterization (*2*), because it directly measures both the amplitude $E(\omega)$ and phase $\phi(\omega)$ of electromagnetic radiation over a broad range of frequencies, ω, thereby allowing straightforward extraction of a material's complex dielectric properties. The pulsed nature of the technique also allows tomographic three-dimensional (3D) spatial mapping of dielectric properties of materials using a methodology similar to radar. Such spectral imaging is nondestructive and has been applied in a wide range of applications including pharmaceutical quality control, medical diagnostics, and production-line inspection. Furthermore, the pulsed nature of the TDS technique facilitates studying dynamic processes in materials with femtosecond time resolution (*3*, *4*).

The vast majority of THz-TDS systems are based on generation and detection of a linearly polarized component of single-cycle THz pulses. In the frequency domain, such data may be represented as $E(\omega)e^{i\phi(\omega)}$, where the two parameters $E(\omega)$ and $\phi(\omega)$ are the amplitude and phase spectra, respectively. Yet, a complete description of a THz pulse must also specify its polarization, which requires two additional parameters to describe the frequency dependence of polarization angle and ellipticity. So, formally the full state of a THz pulse may be described by a 4D Stokes vector or Jones vector for each frequency component of its broad spectrum (*5*). Thus, by encoding polarization information on a THz pulse, it is theoretically possible to double the information it transmits. In spectroscopy, measuring the full state of THz radiation facilitates extraction of anisotropic dielectric properties of materials (which could be affected by surface topography, crystal structure, stress, and magnetic fields) and is key to new techniques such as the THz optical-Hall effect (*6*), THz ellipsometry (*7*), and vibrational circular dichroism spectroscopy (*8*). In THz pulsed imaging applications, polarization information enables high-resolution THz tomography and helps correct the artifacts associated with birefringence and scattering from sample edges (*9*). Therefore, the capability of polarization measurement with THz-TDS is in high demand. Indeed, polarization-resolved THz-TDS systems have been demonstrated since the late 1990s (*10*). However, a lack of measurement schemes for fast and precise polarization sensing has impeded their applications. Currently, polarization detection with THz-TDS can be realized using wire-grid THz polarizers, rotatable polarized THz sources (*11*, *12*), or polarization-sensitive detectors (*13*, *14*).

In most cases, only one component of the THz electric field vector can be measured over

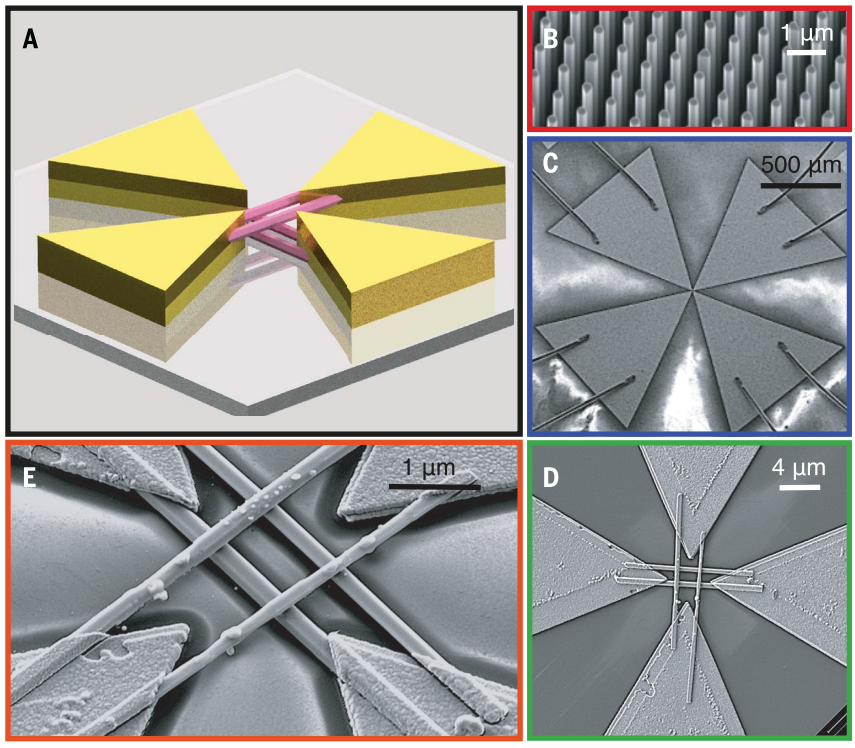

Fig. 1. Structure of the polarization-sensitive cross-nanowire THz detector. (**A**) Schematic illustration of device geometry. (**B**) Scanning electron micrograph (SEM) image of the as-grown InP nanowire array. (**C** to **E**) SEM images of the fabricated detector (blue: entire device; green: center of device; orange: close-up center of device under a tilted view of 25°).

[1]Department of Physics, University of Oxford, Clarendon Laboratory, Oxford OX1 3PU, UK. [2]Institute of Photonics, SUPA Department of Physics, University of Strathclyde, Technology and Innovation Centre, 99 George Street, Glasgow G1 1RD, UK. [3]Department of Electronic Materials Engineering, Research School of Physics, The Australian National University, Canberra, ACT 2601, Australia.
*Corresponding author. Email: michael.johnston@physics.ox.ac.uk

one time-domain scan. For determining the full polarization state, doubled data acquisition time is required, which is problematic for mapping and imaging applications. The use of a multicontact photoconductive antenna (*15*–*17*) for polarization-sensitive measurement is an exceptional case, because this detector type can simultaneously measure the THz electric field vector along multiple directions during a single time-domain scan. However, these devices are difficult to align and cross-talk between detection channels complicates extraction of the polarization state (*15*, *18*), thereby limiting their practical use. Seemingly, the field has reached a technological plateau, calling for a new approach. In this Report, we propose and demonstrate an innovative detector design that uses nanotechnology to measure THz polarization in full. The detector is alignment insensitive and free from the cross-talk, suggesting an ease of implementation in both scientific and industrial settings.

The active elements in our detector are single-crystal semiconductor nanowires that have been systemically studied in our previous work (*19*–*21*) confirming their good suitability for photoconductive THz detection. Here we used indium phosphide (InP) nanowires with a pure wurtzite crystal structure and an approximate average diameter and length of 280 nm and 10 μm, respectively (see materials and methods MM1). The detector architecture is shown in Fig. 1 and consists of two orthogonal gold bow-tie electrodes that are separately bridged by well-aligned nanowires in a "hashtag" configuration. The nanowires on each bow-tie electrode are parallel to the gap orientation, and thus the nanowires contacted by different bow-tie electrodes are orthogonal while being spatially separated perpendicular to the substrate to ensure that they are electrically isolated.

The device architecture was inspired by our previous findings that both single semiconductor nanowires (*22*) and bow-tie THz detectors exhibit extremely high polarization selectivity to absorption of both THz radiation and above-bandgap light. Thus, bow-tie THz detectors based on orthogonal semiconductor nanowires should offer little electromagnetic interference between polarization channels, making them perfect for full polarization characterization.

The cross-nanowire devices were realized through two steps of electron beam lithography and nanowire micropositioning using a "transfer print" technique to effectively manipulate the nanowire location and orientation in the device (see MM2 and MM3), enabling the creation of electrically isolated orthogonal polarization detection channels, thereby avoiding electrical cross-talk. In this work, we concentrate on a hashtag device design with a pair of nanowires per channel. However, the numbers of nanowires for each electrode can be altered; for example, a structure with a single nanowire per channel is presented in fig. S3.

After fabrication, the polarization-sensitive cross-nanowire detectors were characterized in a custom-built THz-TDS system (see MM4 and MM5). Briefly, each near-infrared pulse from a femtosecond laser was split into two: one used to generate a linearly polarized THz pulse in a THz emitter and the other to photoexcite electrons and holes in the cross-nanowire detector. The THz pulse from the emitter was focused on the detector, inducing a transient photocurrent (proportional to the THz field) in each detection channel, which was recorded as a function of time delay t between the THz pulse and optical pulse. The electric-field component of the THz pulse polarized parallel to each antenna (electrode) caused current to flow along its nanowires only after photoexcitation (*23*). Thus, to recover the electric field of the THz pulse in the time domain, the photocurrent data for each channel were differentiated as a function of t (see supplementary text ST1) (*24*). Frequency-domain data were obtained by Fourier transform of the time-domain data.

First, the spectral response of our nanowire detector was examined as shown in Fig. 2A. It can be seen clearly that the horizontal and vertical channels produced responses simultaneously with a current level of a few picoamps, spectral bandwidth of ~2 THz (defined as the cut-off frequency at the noise floor of the frequency spectrum), and low-noise performance, which are consistent with our earlier work (*20*). The current generated by the hashtag detector is limited by the nanosized active material volume but can be increased by adding more nanowires to the array or using larger-diameter nanowires. The two orthogonal channels have a strong linear response relative to the incident THz polarization, where the response current reaches

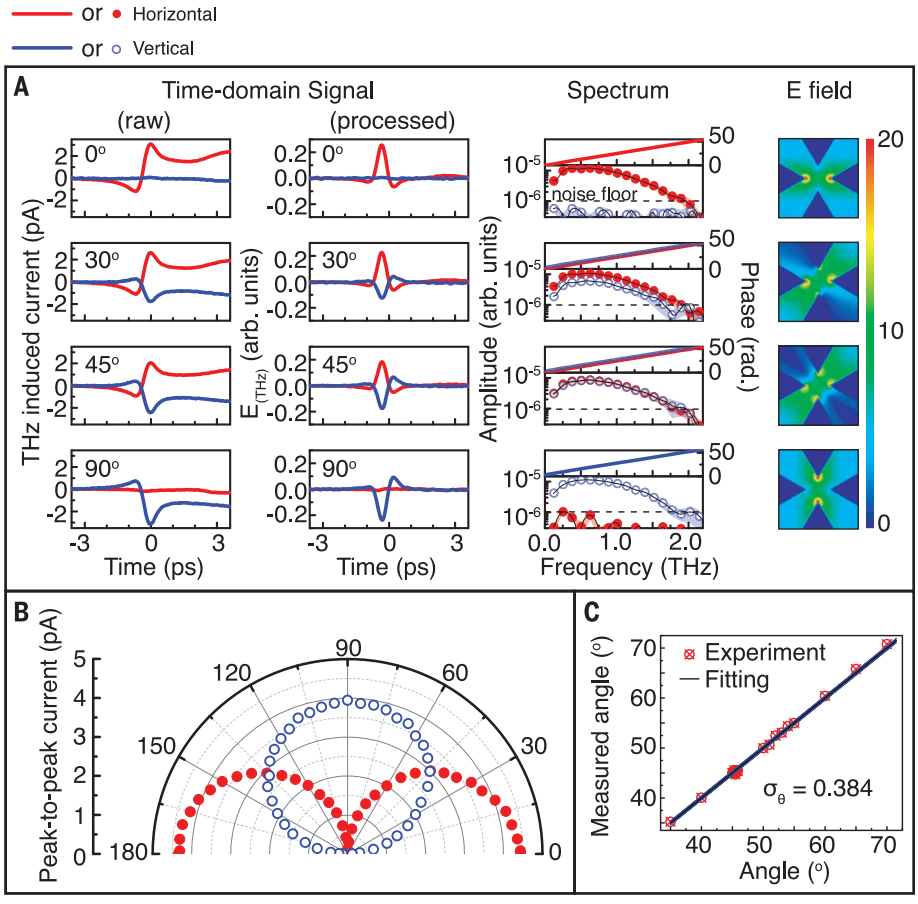

Fig. 2. Characterization of the polarization-sensitive cross-nanowire detector in THz-TDS. (**A**) Responses of the nanowire detector relative to the incident THz polarization (left: raw and processed time-domain THz electric field; middle: amplitude and phase spectrum of the THz electric field; right: simulated THz electric field distribution at 1 THz). 0°, 30°, 60°, and 90° are the angles at which the incident THz pulse is polarized. Red solid line: response from the horizontal-detection channel; blue solid line: response from the vertical-detection channel. (**B**) Relationship between the two orthogonal detection channels in the nanowire detector as a function of the incident THz polarization. Red dots: response from the horizontal-detection channel; blue circles: response from the vertical-detection channel. (**C**) Relative changes of the THz polarization measured by the nanowire detector (cross-circles) for different emitter rotation angles.

a maximum when the THz pulse is polarized parallel to the channel orientation and drops to nearly zero when polarized perpendicular to the channel orientation.

Finite-difference time-domain simulations (FDTDs) were performed to examine the electrode response to the incident THz polarization, which is also linear for each bow-tie structure (see Fig. 2A). The bow-tie antenna structure enhances the intrinsic THz-polarization sensitivity of the nanowires and collects the THz electric field over a much larger area (and concentrates it at the antenna center). Figure 2B illustrates more detailed angle-dependence responses (peak-to-peak current) of both orthogonal detection channels relative to the THz polarization, in excellent agreement with expected cosine and sine functions. This indicates that the two orthogonal channels are independent without any measurable cross-talk between them.

For comparison, we fabricated a multicontact photoconductive antenna, which had the same electrode structure as used in our nanowire detector but used a more conventional Fe^{+}-implanted InP substrate as the active material. This bulk reference device was measured under conditions identical to those for the nanowire detector. As expected, strong cross-talk dominates the signal and furthermore the degree of cross-talk is dependent on the size and position of the optical excitation spot (see ST3), making extraction of the THz polarization state nontrivial and alignment dependent.

The polarization selectivity of each channel of the nanowire hashtag detector was assessed by measuring the cross-polarized THz extinction ratio. This ratio was found to be 2500 (in power) for the horizontal channel (1440 for the vertical channel), which is a substantial improvement over the ratio of 256 in (*16*) and 108 reported in (*17*) (further analysis is provided in ST3). The high extinction ratio achieved by our hashtag detector is expected, as the aligned nanowires used in our detector are intrinsically polarization sensitive and cross-talk free. After the calibration (see ST4), we assessed the detector sensitivity to the change of the incident THz polarization angle as shown in Fig. 2C. The standard deviation of the measured angle values (calculated from the two-channel data) is 0.38°, indicating that the minimum detectable change of polarization angle is less than 0.4° for our nanowire detector.

To demonstrate the versatility of a polarization-resolved THz-TDS system equipped by our nanowire detector, we characterized a THz metamaterial. Metamaterials for the THz band have attracted considerable attention because of their simplicity of design and capability of manipulating the polarization state of THz radiation (*25*), which is difficult to achieve in natural materials. Here we studied a metamaterial (twisted split-ring resonator pair) that functions as a polarization converter. The schematic illustration of our measurement is shown in Fig. 3A, and the morphology of the metamaterial is presented in Fig. 3B (see MM7). When a linearly polarized THz pulse is transmitted through the metamaterial, a coupling effect will induce co- and cross-polarization components in the transmission direction. FDTD simulations were performed to examine the coupling effect for comparison with experimental results. The simulated and transmission amplitude spectra measured with the hashtag detector are compared in Fig. 3C and show excellent agreement. In particular, the copolarized transmission has a resonance splitting feature (at 1.06 and 1.4 THz) that is also observed in the measured spectra. The difference in the transmission ratio could be attributed to imperfect experimental conditions and/or the dielectric properties of the materials being slightly different from the values used in the simulation. A measurement on a similar metamaterial type has been reported (*26*), where

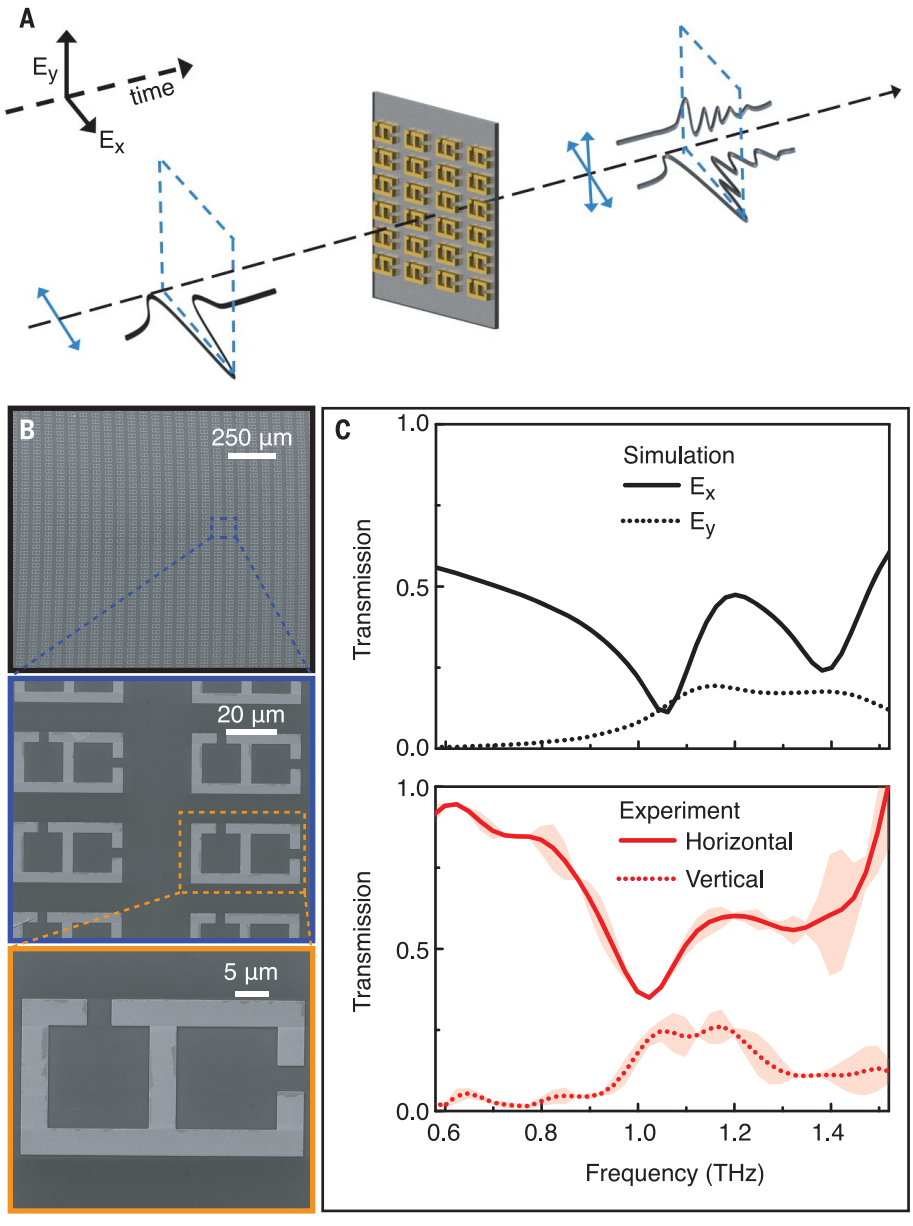

Fig. 3. Application demonstration of polarization-sensitive cross-nanowire detector. (**A**) Schematic representation of transmission measurement of a THz metamaterial. The arrowed blue solid lines show the polarization of the THz pulse before and after passing through the metamaterial. (**B**) SEM images of the fabricated metamaterial. (**C**) Simulated and measured transmission spectra of the THz metamaterial in co- (solid line) and cross- (dotted line) polarizations. Shaded area is the error bar showing the standard variation of repeats in the same measurement.

four wire-grid THz polarizers were used in the system. Our system just required a single scan while providing high polarization accuracy.

In this study, we used orthogonally crossed nanowire networks to develop an ultrafast detector capable of recording the full polarization state of THz radiation and demonstrated its capabilities in the characterization of metamaterials. The monolithic hashtag device is compact and can immediately replace conventional photoconductive receivers in most THz-TDS spectrometers and imaging systems, without any change to the optical layout while vastly improving the capabilities of such systems by including additional spectral polarization information without increased acquisition time. The detector architecture is simple and universal, so any quasi-1D semiconductor nanostructures (e.g., nanorods and nanopillars) could be exploited for further optimization of device performance, in terms of signal-to-noise ratio and accessing ultrabroad spectral bandwidth, thus paving the way to high-speed, high-accuracy THz pulsed imaging. Fast parallel data acquisition for far-field spectral imaging could also be achieved by forming arrays of the hashtag detectors. Furthermore, the detector concept could be scaled down as subwavelength detection units in near-field THz imaging systems for polarization-based super resolution (i.e., nanoscale spatial resolution), or use as an on-chip THz-TDS spectrometer. Therefore, the capabilities and geometry of the detector and its associated on-chip technologies open up a wide range of new scientific applications spanning physics, biology, chemistry, and engineering, while potentially enabling new approaches to industrial quality control, security imaging, and high-speed communications.

REFERENCES AND NOTES

1. S. Dhillon *et al.*, *J. Phys. D Appl. Phys.* **50**, 043001 (2017).
2. B. Ferguson, X. C. Zhang, *Nat. Mater.* **1**, 26–33 (2002).
3. C. Riek *et al.*, *Science* **350**, 420–423 (2015).
4. S. Schlauderer *et al.*, *Nature* **569**, 383–387 (2019).
5. E. Castro-Camus, M. B. Johnston, *J. Opt. A, Pure Appl. Opt.* **11**, 105206 (2009).
6. D. M. Mittleman, J. Cunningham, M. C. Nuss, M. Geva, *Appl. Phys. Lett.* **71**, 16–18 (1997).
7. K. N. Okada *et al.*, *Nat. Commun.* **7**, 12245 (2016).
8. W. J. Choi *et al.*, *Nat. Mater.* **18**, 820–826 (2019).
9. S. Watanabe, *Photonics* **5**, 58 (2018).
10. B. B. Hu, M. C. Nuss, *Opt. Lett.* **20**, 1716–1718 (1995).
11. Q. Chen, X. C. Zhang, *Appl. Phys. Lett.* **74**, 3435–3437 (1999).
12. C. D. W. Mosley, M. Failla, D. Prabhakaran, J. Lloyd-Hughes, *Sci. Rep.* **7**, 12337 (2017).
13. E. Castro-Camus *et al.*, *Opt. Express* **15**, 7047–7057 (2007).
14. N. Nemoto, T. Higuchi, N. Kanda, K. Konishi, M. Kuwata-Gonokami, *Opt. Express* **22**, 17915–17929 (2014).
15. D. S. Bulgarevich *et al.*, *Opt. Express* **22**, 10332–10340 (2014).
16. A. Hussain, S. R. Andrews, *Opt. Express* **16**, 7251–7257 (2008).
17. E. Castro-Camus *et al.*, *Appl. Phys. Lett.* **86**, 254102 (2005).
18. G. Niehues *et al.*, *Opt. Express* **23**, 16184–16195 (2015).
19. K. Peng *et al.*, *Nanotechnology* **28**, 125202 (2017).
20. K. Peng *et al.*, *Nano Lett.* **16**, 4925–4931 (2016).
21. K. Peng *et al.*, *Nano Lett.* **15**, 206–210 (2015).
22. S. A. Baig *et al.*, *Nano Lett.* **17**, 2603–2610 (2017).
23. Z. Yang *et al.*, *Science* **365**, 1017–1020 (2019).
24. E. Castro-Camus *et al.*, *J. Appl. Phys.* **104**, 053113 (2008).
25. T. J. Yen *et al.*, *Science* **303**, 1494–1496 (2004).
26. C. Li, C. C. Chang, Q. Zhou, C. Zhang, H. T. Chen, *Opt. Express* **25**, 25842–25852 (2017).

ACKNOWLEDGMENTS

We thank J. Liu, X. Bian, P. Pattinson, P. Parkinson, and M. Zerbini for useful discussions. We acknowledge the Australian National Fabrication Facility, ACT node (ANFF-ACT), for access to the facilities. Thanks to Z. Li's arrangement, simulation was undertaken with the assistance of resources from the National Computational Infrastructure (NCI Australia). **Funding:** This work was supported by the EPSRC (EP/M017095/1, EP/P006329/1, EP/R034804/1, EP/P013597/1 & EP/R03480X/1), ARC (Australia), and the European Union's Horizon 2020 research and innovation program under grant agreements 735008 (SiLAS) and 828841 (ChipAI). **Author contributions:** M.B.J. conceived the device concept. M.B.J., C.J., and L.F. established this project. K.P. worked on device design, fabrication, characterization, and simulation. D.J., B.G., M.J.S., M.D.D., and A.H. developed the transfer printing technique for the integration of nanowires. D.J. performed the transfer-print process under the supervision of AH. F.Z., L.F., and H.H.T. created the nanowires and ion-implanted wafers. S.S. characterized nanowire photoconductivity. D.A.D. assisted with the fabrication and system optimization. M.U.R. performed scanning electron microscopy under the supervision of L.M.H. K.P. and M.B.J. prepared the manuscript. All authors discussed and commented on the manuscript. **Competing interests:** M.B.J. and K.P. are inventors on UK patent application 2002340.7 submitted by Oxford University that covers the cross-nanowire device concept. **Data and materials availability:** All data needed to reach the conclusions of this Report are presented in the main text or the supplementary materials.

SUPPLEMENTARY MATERIALS

science.sciencemag.org/content/368/6490/510/suppl/DC1
Materials and Methods
Supplementary Text
Figs. S1 to S13
References (*27*–*29*)

29 January 2020; accepted 1 April 2020
10.1126/science.abb0924

Three-dimensional cross-nanowire networks recover full terahertz state

Kun Peng, Dimitars Jevtics, Fanlu Zhang, Sabrina Sterzl, Djamshid A. Damry, Mathias U. Rothmann, Benoit Guilhabert, Michael J. Strain, Hark H. Tan, Laura M. Herz, Lan Fu, Martin D. Dawson, Antonio Hurtado, Chennupati Jagadish and Michael B. Johnston

Science **368** (6490), 510-513.
DOI: 10.1126/science.abb0924

Nanowire-based THz detection

Terahertz (THz) radiation is an interesting region of the electromagnetic spectrum lying between microwaves and infrared. Non-ionizing and transparent to most fabrics, it is finding application in security screening and imaging but is also being developed for communication and chemical sensing. To date, most THz detectors have focused just on signal intensity, an effort that discards half the signal in terms of the full optical state, including polarization. Peng *et al.* developed a THz detector based on crossed nanowires (arranged in a hash structure) that is capable of resolving the full state of the THz light. The approach provides a nanophotonic platform for the further development of THz-based technologies.

Science, this issue p. 510